Robustness Analysis of Long-Horizon Direct Model Predictive Control: Permanent Magnet Synchronous Motor Drives

Ludovico Ortombina
Dep. of Industrial Engineering
University of Padova
Padova, Italy
ludovico.ortombina@unipd.it

Petros Karamanakos
Fac. of Informat. Techn. and Commun. Sciences
Tampere University
Tampere, Finland
p.karamanakos@ieee.org

Mauro Zigliotto
Dep. of Management and Engineering
University of Padova
Padova, Italy
mauro.zigliotto@unipd.it

***Abstract*—Model predictive control (MPC) lacks an integrating element. Thus, parameter mismatches can deteriorate its steady-state performance. To address this issue and enhance the robustness of MPC, an alternative formulation of the prediction model is discussed in this paper. This model introduces an integrator to the optimization problem without increasing its size and consequently its computational complexity. An in-depth analysis of the effect of parameter mismatches on the control performance is performed when both the conventional and the proposed prediction model are used. Specifically, the aforementioned analysis is carried out for a range of switching frequencies as well as prediction horizon lengths, while a permanent magnet synchronous motor (PMSM) drive is used as a case study.**

***Index Terms*—model predictive control (MPC), permanent magnet synchronous machine (PMSM), robustness, parameter sensitivity**

I. Introduction

With the advent of powerful microprocessors, model predictive control (MPC) has been gaining a lot of attention in the field of power electronics in recent years, especially in its version as direct controller, i.e., MPC without a modulator [1], [2]. Among the most attractive characteristics of direct MPC (also known as finite control set MPC—FCS MPC) is its capability to control nonlinear multi-input multi-output systems and to fully exploit the available hardware. At the same time, permanent magnet synchronous motors (PMSMs) are entering new markets, such as traction and automotive applications, electrical mobility, more electric aircrafts, renewable power generation, and home appliances [3]. Their increasing success is due to the highest torque density and efficiency among other electrical machines. Because of this, both academy and industry are investigating effective control schemes that can exploit all PMSM characteristics and MPC seems to be a compelling solution.

As its name implies, MPC is a model-based controller. Hence, the accuracy of the system model—upon which the prediction of the plant behavior depends—is of paramount importance, since an inaccurate prediction model will adversely affect the system performance. Such degradation is even more pronounced when long-horizon MPC is employed. Note that the latter is required to improve performance metrics, such as the load current total harmonic distortion (THD) [4]. Since, however, parameter mismatches are always present, e.g., due to estimation errors, aging, temperature variations, and the variability in the manufacturing process, an in-depth study of how discrepancies between the prediction and actual system model affect the closed-loop behavior of MPC needs to be done.

MPC robustness against modeling uncertainties can be addressed in two ways, namely, by modifying the control scheme, or by improving the parameter estimation. Several methods belong to the former category. For instance, [5] proposed a new cost function with an integral term of the current tracking error, while [6] added a weighted error to the *dq*–predicted currents which was computed among the predicted current and the measured one at the last switching instant. An alternative was presented in [7] where the system state was augmented to include an explicit integrator. It is worth noting that most of the aforementioned techniques, rely on the addition of an integrator to the optimization problem since MPC is merely a proportional controller [8]. On the other hand, detrimental parameter mismatch effects on the control performance can be mitigated by tracking the motor parameters during the normal motor operation, as, e.g., in [9], [10]. Moreover, a gray box approach can be chosen [11] where an equivalent motor model is implemented and its parameters are estimated and updated in real time by means of the measured motor quantities, i.e., currents, voltages and speed.

A step preceding the development of a control technique, or the implementation of an estimation method should be the analysis of the influence of each parameter on the control performance. The reason is that it is crucial to understand which is the parameter that mainly affects the control performance so that effort can be put into mitigating it. [12] studied the influence of resistance and/or inductance mismatches in a generic voltage–source converter. It showed how the parameter sensitivity changes as a function of the load current and a comparison with a proportional–integral control

is reported. In [13] a PMSM was analyzed and an incremental prediction *dq*–model was proposed which was insensitive to the permanent magnet (PM) mismatches; this, however was not experimentally showed. Moreover, both above-mentioned works considered only a single–step horizon, while the ℓ_1–norm—which has detrimental effect on MPC stability and performance—was used [14].

Based on the above, in this paper, the robustness of FCS–MPC to parameter mismatches using a PMSM drive as a case study. At first, the classical MPC formulation is reported and the effects of discrepancy of parameters, such as the stator resistance, the inductance and the PM flux, on the current tracking accuracy of MPC and current THD are investigated. To this aim, different degrees of (both positive and negative) parameter mismatch and prediction horizon lengths are examined. Following, to attenuate the adverse effects of parameter mismatches on the control performance, an alternative prediction model is proposed which introduces an integrator to the control strategy [15]–[17]. It is noteworthy that in doing so, the size, and thus the complexity, of the optimization problem remain constant. To obtain the optimal control solution the proposed formulation computes the variation of the control action and integrates it starting from the action applied last. The performance and the robustness of the presented strategy are compared with those of the classical FCS-MPC formulation in the most critical situation for each motor parameter, namely with a significant mismatch and long prediction horizon.

II. Physical Model of the System

The system under consideration consists of a three-level neutral point clamped (NPC) voltage source inverter and a PMSM. The dc-link voltage of the inverter V_{dc} is assumed to be constant and the neutral point potential v_N is fixed to zero.

The modeling and the control formulation are done in the orthogonal $\alpha\beta$–reference frame. To do so, three-phase (abc) variables in the form $\boldsymbol{\xi}_{abc} = [\xi_a \ \xi_b \ \xi_c]^T$ are transformed into two-dimensional variables $\boldsymbol{\xi}_{\alpha\beta} = [\xi_\alpha \ \xi_\beta]^T$ in the stationary ($\alpha\beta$) reference frame via $\boldsymbol{\xi}_{\alpha\beta} = \mathbf{K}\boldsymbol{\xi}_{abc}$, where $\mathbf{K}$ is the Clarke transformation matrix

$$\mathbf{K} = \frac{2}{3}\begin{bmatrix} 1 & -\frac{1}{2} & -\frac{1}{2} \\ 0 & \frac{\sqrt{3}}{2} & -\frac{\sqrt{3}}{2} \end{bmatrix}. \tag{1}$$

Through the paper, the quantities are normalized and presented in the per unit (p.u.) system.

First, the inverter model is derived. A three-level NPC inverter can produce the phase voltages $-V_{\text{dc}}/2$, 0, and $V_{\text{dc}}/2$, depending on the switch position on the corresponding phase. The latter can be represented by the integer variables $u_a, u_b, u_c \in \mathcal{U} \triangleq \{-1, 0, 1\}$, which can be aggregated to the three-phase switch position $\boldsymbol{u}_{abc} = [u_a \ u_b \ u_c]^T \in \boldsymbol{\mathcal{U}} \triangleq \mathcal{U}^3$.

In the next step, the state–space model of the controlled PMSM is derived. The motor voltage equation in the stationary reference frame is

$$\boldsymbol{v}_{\alpha\beta} = R\boldsymbol{i}_{\alpha\beta} + X_s\frac{\mathrm{d}\boldsymbol{i}_{\alpha\beta}}{\mathrm{d}t} + \omega_{\text{me}}\Psi_{\text{mg}}[-\sin(\theta_{\text{me}}) \ \cos(\theta_{\text{me}})]^T \tag{2}$$

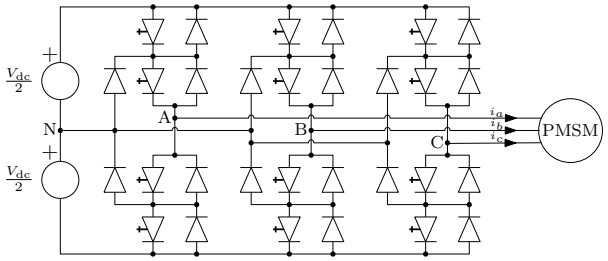

Fig. 1: Three-level NPC voltage source inverter with a PMSM. The inverter has a fixed neutral point potential.

where $\boldsymbol{v}_{\alpha\beta} = [v_\alpha \ v_\beta]^T$, and $\boldsymbol{i}_{\alpha\beta} = [i_\alpha \ i_\beta]^T$ are the stator voltage and current, respectively, Ψ_{mg} the PM flux linkage, R and X_s the stator resistance and reactance, respectively, θ_{me} the electromechanical position, and ω_{me} the electromechanical speed. For sake of simplicity, the mechanical dynamics are neglected by adopting the infinite inertia hypothesis, leading to a constant motor speed during a current control cycle.

Since MPC is discrete-time controller the discretization of the continuous-time PMSM model is required. To this end, forward Euler discretization is employed and applied to (2), yielding the discrete–time PMSM model, i.e.,

$$\begin{aligned}\boldsymbol{i}_{\alpha\beta}(k+1) &= \left(1 - \frac{T_s R}{X_s}\right)\boldsymbol{i}_{\alpha\beta}(k) + \frac{V_{\text{dc}}}{2}\frac{T_s}{X_s}\mathbf{K}\boldsymbol{u}_{abc}(k) \\ &\quad + \frac{T_s\omega_{\text{me}}(k)}{X_s}\Psi_{\text{mg}}[-\sin(\theta_{\text{me}}(k)) \ \cos(\theta_{\text{me}}(k))]^T \\ &= \mathbf{A}\boldsymbol{i}_{\alpha\beta}(k) + \mathbf{B}\boldsymbol{u}_{abc}(k) + \boldsymbol{d}(k)\end{aligned} \tag{3}$$

where the matrices $\mathbf{A}$, $\mathbf{B}$ and $\boldsymbol{d}$ definition can be devised by the previous equation, T_s is the sampling interval and $k \in \mathbb{N}$. Finally, it is worth noting that matrices $\mathbf{A}$ and $\mathbf{B}$ are assumed to be time invariant, while vector $\boldsymbol{d}(k)$ is time varying.

III. Direct Model Predictive Control with Reference Tracking

The direct MPC is a control paradigm which directly chooses the position of the inverter switches, namely $\boldsymbol{u}_{abc}$, while avoiding the use of a modulator. The controller predicts for N_p time steps the future evolution of the controlled variables on the basis of the system model and the candidate sequences of control actions, i.e., switching sequences. The optimal control action corresponds to the switching sequence that minimizes a predetermined performance index, referred to as *cost function. This quantifies* the control requirements, which, for the chosen case study, i.e., a PMSM drive system, are twofold, namely, the regulation of the stator current along its reference and the operation at as a low switching frequency as possible for reduced power losses. These objectives can be mapped into a scalar via the following cost function

$$J(k) = \sum_{\ell=k}^{k+N_p-1} \|\boldsymbol{i}_{\text{err},\alpha\beta}(\ell+1)\|_2^2 + \lambda_u \|\Delta\boldsymbol{u}_{abc}(\ell)\|_2^2 \tag{4}$$

which considers the weighted sum of the current tracking error defined as $\boldsymbol{i}_{\text{err},\alpha\beta}(\ell) = \boldsymbol{i}_{\text{ref},\alpha\beta}(\ell) - \boldsymbol{i}_{\alpha\beta}(\ell)$. Moreover,

$\Delta \boldsymbol{u}_{abc}(\ell) \triangleq \boldsymbol{u}_{abc}(\ell) - \boldsymbol{u}_{abc}(\ell-1)$ takes into account the switching transitions involved between two consecutive time steps. The weighting factor $\lambda_u > 0$ decides on the trade-off between the current tracking accuracy and the switching losses (i.e., switching frequency).

To find the optimal sequence of switch positions over the prediction horizon N_p, i.e., $\mathbf{U}^*(k) = [\boldsymbol{u}_{abc}^{*T}(k)\ \boldsymbol{u}_{abc}^{*T}(k+1)\ \dots\ \boldsymbol{u}_{abc}^{*T}(k+N_p-1)]^T$, problem

$$\begin{aligned} \mathbf{U}^*(k) = &\arg \underset{\mathbf{U}_k}{\text{minimize}}\ J(k) \\ \text{subject to } &\boldsymbol{i}_{\alpha\beta}(\ell+1) = \mathbf{A}\boldsymbol{i}_{\alpha\beta}(\ell) + \mathbf{B}\boldsymbol{u}_{abc}(\ell) + \boldsymbol{d}(\ell) \\ &\mathbf{U}_k \in \mathbb{U} \\ &\left\|\Delta \boldsymbol{u}_{abc}(l)\right\|_\infty \leq 1,\ \forall \ell = k, \cdots, k+N_p-1 \end{aligned} \tag{5}$$

must be solved in real time. In (5), $\mathbf{U}(k) = [\boldsymbol{u}_{abc}^{T}(k)\ \boldsymbol{u}_{abc}^{T}(k+1)\ \dots\ \boldsymbol{u}_{abc}^{T}(k+N_p-1)]^T$ is the optimization variable and $\mathbb{U} = \boldsymbol{\mathcal{U}} \times \dots \times \boldsymbol{\mathcal{U}}$ is the N_p–times Cartesian product of the set $\boldsymbol{\mathcal{U}}$ and represents the feasible input set.

To solve the integer optimization problem (5) in a computationally efficient manner, i.e., to reduce the number of candidate solutions that need to be evaluated in real time, further manipulations are required. The aim is to employ smart branch–and–bound algorithms, such as the sphere decoding algorithm (SDA) [18]. To this end, the unconstrained solution of (5) needs to be computed first. To do so, the algorithm in [18] is slightly modified to account for the exogenous disturbance $\boldsymbol{d}(k)$ in (3). For this, it is enough to note that the vector $\boldsymbol{d}(k)$ is fully described by the electromechanical position and speed. Thanks to the infinite inertia hypothesis, $\boldsymbol{d}(k)$ can be easily predicted for N_p steps by keeping the electromechanical speed constant and updating the rotor position as $\theta_{\text{me}}(k+\ell) = \theta_{\text{me}}(k) + \omega_{\text{me}}\ell T_s$ with $\ell = 0, \dots, N_p - 1$. Hence, the unconstrained solution $\mathbf{U}_{\text{unc}}(k)$ can be computed as

$$\mathbf{U}_{\text{unc}}(k) = \mathbf{H}^{-1}\boldsymbol{\Theta}^T(k) \tag{6}$$

where

$$\begin{aligned} \mathbf{H} &= \boldsymbol{\Upsilon}^T\boldsymbol{\Upsilon} + \lambda_u \mathbf{S}^T\mathbf{S} \\ \boldsymbol{\Theta}(k) &= \left(\mathbf{Y}_{\text{ref}}(k) - \boldsymbol{\Gamma}\boldsymbol{i}_{\alpha\beta}(k) - \mathbf{M}\mathbf{D}(k)\right)^T \boldsymbol{\Upsilon} \\ &\quad + \lambda_u \left(\mathbf{E}\boldsymbol{u}_{abc}^*(k)\right)^T \mathbf{S}\,. \end{aligned} \tag{7}$$

In (7), $\mathbf{Y}_{\text{ref}}(k)$ is the reference current over the prediction horizon $\mathbf{Y}_{\text{ref}}(k) = \left[\boldsymbol{i}_{\text{ref},\alpha\beta}^T(k+1)\ \boldsymbol{i}_{\text{ref},\alpha\beta}^T(k+2)\ \dots\ \boldsymbol{i}_{\text{ref},\alpha\beta}^T(k+N_p)\right]^T$, while all matrices are defined in the appendix.

With (6), the MPC problem (5) can be written as

$$\begin{aligned} \mathbf{U}^*(k) = &\arg \underset{\mathbf{U}_k}{\text{minimize}}\ \left\|\bar{\mathbf{U}}_{\text{unc}} - \mathbf{V}\mathbf{U}(k)\right\|_2^2 \\ \text{subject to } &\mathbf{U}_k \in \mathbb{U} \\ &\left\|\Delta \boldsymbol{u}_{abc}(l)\right\|_\infty \leq 1,\ \forall \ell = k, \cdots, k+N_p-1 \end{aligned} \tag{8}$$

where it holds that $\mathbf{V}^T\mathbf{V} = \mathbf{H}$ with $\mathbf{V}$ being a nonsingular lower triangular matrix provided that $\lambda_u > 0$. Moreover, $\bar{\mathbf{U}}_{\text{unc}} = \mathbf{V}\mathbf{U}_{\text{unc}}$.

Problem (8) describes the integer least-squares (ILS) problem solved in [18]. This can be interpreted as the minimization of the hypersphere of radius ρ (i.e., the value of the cost function) centered at $\mathbf{U}_{\text{unc}}(k)$. The SDA evaluates only the candidate solutions inside the computed hypersphere and the one that returns the smallest cost function value is the optimal one. Specifically, the solution $\mathbf{U}^*(k)$ corresponds to the n–dimensional lattice point with the smallest Euclidean distance from the unconstrained solution $\bar{\mathbf{U}}_{\text{unc}}$. Equivalently, the solution is the unique lattice point included in the smallest hypersphere centered at $\bar{\mathbf{U}}_{\text{unc}}$ of radius ρ. It is worth noting that SDA still guarantees optimality with a highly computational efficiency, especially if compared with the brute–force approach of the exhaustive enumeration.

As can be understood, the initial choice of the radius ρ plays a crucial role in the SDA efficiency. The hypersphere must be as small as possible to evaluate a small number of nodes, but it should not be empty to ensure that a solution is found. The initial radius can be set as proposed in [19], i.e.,

$$\rho = \min\left\{\rho_a,\, \rho_b\right\} \tag{9}$$

where

$$\rho_a = \left\|\bar{\mathbf{U}}_{\text{unc}} - \mathbf{V}\mathbf{U}_{\text{bab}}(k)\right\|_2 \tag{10a}$$

$$\rho_b = \left\|\bar{\mathbf{U}}_{\text{unc}} - \mathbf{V}\mathbf{U}_{\text{ed}}(k)\right\|_2. \tag{10b}$$

The radii in (10) are computed based on two different possibilities, namely the so–called Babai estimate $\mathbf{U}_{\text{bab}}$ or the educational guess $\mathbf{U}_{\text{ed}}$. The former solution corresponds to the rounded unconstrained solution to the closest integer vector, i.e., $\mathbf{U}_{\text{bab}}(k) = \lfloor \mathbf{U}_{\text{unc}}(k) \rceil$, while the latter is the previously applied optimal solution $\mathbf{U}^*(k-1)$ shifted by one time step.

Once $\mathbf{U}^*(k)$ is found, and in line with the receding horizon policy, only its first element is applied by the converter whereas the rest are discarded. The procedure continues at the next time step over a one time-step shifted horizon and based on new measurements/estimates.

IV. Velocity model

MPC is, essentially, a proportional control method [8]. Hence, its steady-state performance is susceptible to model mismatches, parameter uncertainties, and/or unmodeled disturbances. To address this issue, some techniques have been proposed that add an explicit integrator to the state vector [7], [20]. This, however, increases the dimension of the model, and makes the MPC problem more complex, especially when a long horizon is adopted for improving system performance.

To address the aforementioned issue of the augmented state, a different formulation of the MPC problem is adopted. It is based on the *velocity form* of the model which returns the input variation—or velocity of the control input—instead of the entire control action itself. The control input is subsequently obtained by integrating its velocity [15]–[17].

To derive the velocity model, the state, input and disturbance variations, i.e., $\Delta\boldsymbol{i}_{\alpha\beta}(k) = \boldsymbol{i}_{\alpha\beta}(k) - \boldsymbol{i}_{\alpha\beta}(k-1)$, $\Delta\boldsymbol{u}_{abc}(k) = \boldsymbol{u}_{abc}(k) - \boldsymbol{u}_{abc}(k-1)$, and $\Delta\boldsymbol{d}(k) = \boldsymbol{d}(k) - \boldsymbol{d}(k-1)$,

respectively, are required. With these, the drive model to serve as an internal prediction model for FCS–MPC becomes

$$\begin{aligned}\Delta \boldsymbol{i}_{\alpha\beta}(k+1) &= \boldsymbol{i}_{\alpha\beta}(k+1) - \boldsymbol{i}_{\alpha\beta}(k) \\ &= \mathbf{A}\Delta \boldsymbol{i}_{\alpha\beta}(k) + \mathbf{B}\Delta \boldsymbol{u}_{abc}(k) + \Delta \boldsymbol{d}(k) \end{aligned} \quad (11)$$

which allows to compute the current variation with respect to the measured one. The PMSM velocity form in (11) resembles the classical formulation (3) and it can be used to minimize the cost function (4). Moreover, it is worth highlighting that (11) is well tailored to to the required form of (4) since the input variation $\Delta \boldsymbol{u}_{abc}(k)$ in (11) is the control effort term in (4). On the other hand, the predicted current trajectory is no more directly available since (11) only returns its variation.

Let $\Delta\mathbf{Y}(k+1) = \left[\Delta \boldsymbol{i}_{\alpha\beta}(k+1)^T \ \dots \ \Delta \boldsymbol{i}_{\alpha\beta}(k+N_p)^T\right]^T$, $\Delta\mathbf{U}(k) = \left[\Delta \boldsymbol{u}_{abc}(k)^T \ \dots \ \Delta \boldsymbol{u}_{abc}(k+N_p-1)^T\right]^T$, and $\Delta\mathbf{D}(k) = \left[\Delta \boldsymbol{d}(k)^T \ \dots \ \Delta \boldsymbol{d}(k+N_p-1)^T\right]^T$ be the current, the input and the disturbance variation vectors over the prediction horizon, respectively. The output variation vector can be rearranged as

$$\Delta\mathbf{Y}(k+1) = \mathbf{\Gamma}\Delta \boldsymbol{i}_{\alpha\beta}(k) + \mathbf{\Upsilon}\Delta\mathbf{U} + \mathbf{M}\Delta\mathbf{D}(k) \quad (12)$$

and the entire predicted output current trajectory $\mathbf{Y}(k) = \left[\boldsymbol{i}_{\alpha\beta}(k+1)^T \ \dots \ \boldsymbol{i}_{\alpha\beta}(k+N_p)^T\right]^T$ can be computed by integrating $\Delta\mathbf{Y}(k+1)$ starting from $\boldsymbol{i}_{\alpha\beta}(k)$ as follows

$$\begin{aligned}\mathbf{Y}(k) &= \begin{bmatrix}\boldsymbol{i}_{\alpha\beta}(k)\\ \vdots \\ \boldsymbol{i}_{\alpha\beta}(k)\end{bmatrix} + \begin{bmatrix}\mathbf{I} & \mathbf{0} & \cdots & \mathbf{0}\\ \mathbf{I} & \mathbf{I} & \cdots & \mathbf{0}\\ \vdots & \vdots & & \vdots \\ \mathbf{I} & \mathbf{I} & \cdots & \mathbf{I}\end{bmatrix}\Delta\mathbf{Y}(k+1) \\ &= \bar{\mathbf{Y}}(k) + \mathbf{S}_i\Delta\mathbf{Y}(k+1). \end{aligned} \quad (13)$$

With this, function (4) can be rewritten as

$$J(k) = (\mathbf{Y}_{\text{ref}}(k) - \mathbf{Y}(k))^T(\mathbf{Y}_{\text{ref}}(k) - \mathbf{Y}(k)) + \lambda_u\Delta\mathbf{U}^T\Delta\mathbf{U}. \quad (14)$$

By relaxing the feasible set from $\mathbb{U}$ to $\mathbb{R}^{3N_p}$, and by taking into account the new cost function (14), the unconstrained solution of (5) is

$$\Delta\mathbf{U}_{\text{unc}}(k) = \mathbf{H}_i^{-1}\mathbf{\Theta}_i^T(k) \quad (15)$$

where

$$\begin{aligned}\mathbf{H}_i &= \mathbf{\Upsilon}^T\mathbf{S}_i^T\mathbf{S}_i\mathbf{\Upsilon} + \lambda_u\mathbf{I} \\ \mathbf{\Theta}_i(k) &= \big(\mathbf{Y}_{\text{ref}}(k) - \bar{\mathbf{Y}}(k) \\ &\qquad - \mathbf{S}_i(\mathbf{\Gamma}\Delta \boldsymbol{i}_{\alpha\beta}(k) + \mathbf{M}\Delta\mathbf{D}(k))^T\big)\mathbf{S}_i\mathbf{\Gamma}. \end{aligned} \quad (16)$$

Expression (15) returns the control input variation, thus it must be integrated starting from the last applied switch position $\boldsymbol{u}_{abc}(k-1)$ to compute the entire input unconstrained solution $\mathbf{U}_{\text{unc}}$, i.e.,

$$\mathbf{U}_{\text{unc}} = \bar{\mathbf{U}}(k) + \mathbf{S}_i\Delta\mathbf{U}_{\text{unc}}(k) \quad (17)$$

where $\bar{\mathbf{U}}(k) = \left[\boldsymbol{u}_{abc}^T(k-1) \ \dots \ \boldsymbol{u}_{abc}^T(k-1)\right]^T$. Finally, to solve the optimization problem underlying FCS–MPC in a computationally efficient manner the SDA can be still applied, as in Section III. It is worth remembering that the lattice generator matrix $\mathbf{V}$ remains unchanged. Moreover, matrix $\mathbf{H}$ describes the real physical system, whereas $\mathbf{H}_i$ models the rate of change of the plant.

The proposed formulation adds an integrator to the MPC problem. The unconstrained solution is computed by integrating the variation of the control action, strongly differentiating it from the classical formulation where it is the exact solution of the (unconstrained) problem. Thanks to this, the control scheme changes its behavior against parameter mismatches by showing more robustness to them, as shown in Section V. However, the velocity formulation is equivalent to the classical one without parameters discrepancy. Furthermore, the computational complexity remains the same as that of the original FCS–MPC problem since the Hessian matrices $\mathbf{H}$ and $\mathbf{H}_i$ as well as the vectors $\mathbf{\Theta}$ and $\mathbf{\Theta}_i$ have the same dimensions. This is an important benefit of the proposed modeling, especially when considering that techniques which include an integrator by augmenting the state considerably increase the size of the optimization problem, especially if a long horizon is implemented.

TABLE I: System nameplate data.

Parameter	Nameplate data	p.u.
Rated current (I_R)	10.9 A	1 p.u.
Rated speed (ω_R)	4500 rpm	0.25 p.u.
Rated Torque (τ_R)	10.9 N m	0.9832 p.u.
Pole pairs (p)	4	4
Permanent magnet (Λ_{mg})	0.1667 V s	0.9832 p.u.
Stator resistance (R_s)	240 mΩ	0.0082 p.u.
Stator inductance (X_s)	3.15 mH	0.2025 p.u.
Dc-link voltage (V_{dc})	560 V	1.7146 p.u.

V. Robustness Analysis

The effect of model parameter mismatches on FCS–MPC with conventional prediction model (3) and with the velocity one (11) is presented hereafter. Specifically, it is studied how the system performance is affected by variations in all motor parameters, namely the stator resistance, the stator inductance and the PM flux linkage value, and for different prediction horizons. A mismatch was introduced by varying the value of a parameter in the prediction model, while keeping the same parameter constant in the simulated motor. In order to understand the system robustness, several series of simulations were performed. Table I lists the parameters of the PMSM-based motor drive in both absolute and p.u. values. The sampling interval was set to T_s = 25 µs. All the simulations were carried out at rated speed and load, while $i_{d,\text{ref}} = 0$ p.u. and $i_{q,\text{ref}} = 1$ p.u. were assumed to work in maximum torque per Ampere (MTPA) conditions. As mentioned in Section II, the controller is designed in the $\alpha\beta$-plane. However, in the sequel of this section, for demonstration purposes, and to provide deeper insight, the tracking accuracy of MPC is shown in the dq–plane. Finally, for further insight, the product of current THD (I_{THD}) and switching frequency (f_{sw}), i.e., $c_f = I_{\text{THD}} \cdot f_{\text{sw}}$, serves as a meaningful performance metric [4].

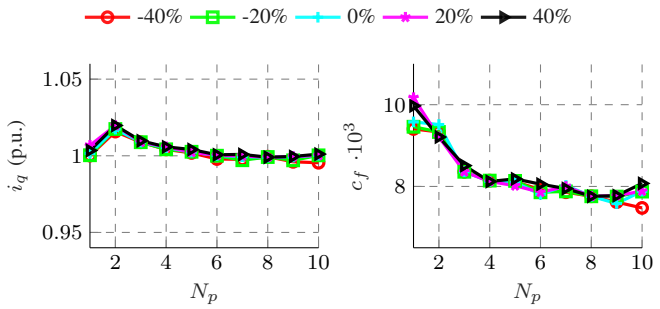

(a) Mean q-current value (b) c_f factor

Fig. 2: Current behavior and c_f as a function of the prediction horizon N_p, when using FCS-MPC with (constant) $\lambda_u = 0.01$ and different degrees of resistance mismatch.

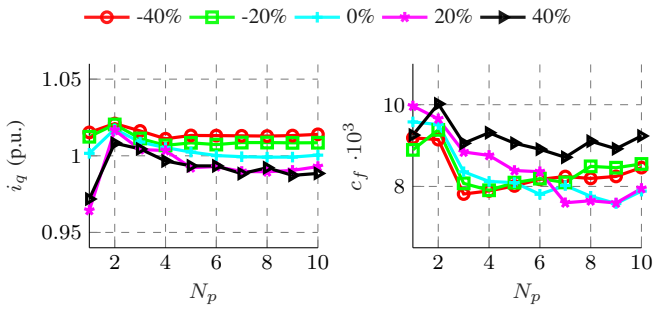

(a) Mean q-current value (b) c_f factor

Fig. 3: Current behaviour and c_f as a function of the prediction horizon N_p, when using FCS-MPC with (constant) $\lambda_u = 0.01$ and different degrees of inductance mismatch.

A. FCS–MPC Based on the Conventional Prediction Model

First, the robustness of FCS–MPC with the conventional prediction model was tested. To this end, different degrees of mismatch are applied to each of the three aforementioned parameters, i.e., the resistance, inductance, and PM, separately and the effect on the MPC performance is shown in Figs. 2, 3, and 4, respectively. The nominal case, namely without any parameter mismatches, is reported as well. Figs. 2a, 3a, and 4a depict the mean q–current value in steady–state condition, while Figs. 2b, 3b, and 4b show the c_f factor for different prediction horizon lengths and $\lambda_u = 0.01$.

1) Resistance Analysis: The stator resistance value is mainly affected by the motor temperature and its value can considerably change during the normal motor operation [21]. To account for this it as well as for the estimation error of the nominal value, mismatches in the range of $\pm 40\%$ of the nominal value were simulated. As can be observed in Fig. 2, the stator resistance has a negligible detrimental effect on the MPC performance regardless of the prediction horizon length. Since at full speed the resistance voltage drop is very small, the prediction error due to a resistance mismatch has a minimal effect on the overall system performance. Moreover, as shown in Fig. 2b, the c_f factor is almost always the same, regardless of the degree of mismatch or length of the horizon.

2) Inductance Analysis: PMSMs are usually characterized by a large equivalent air–gap, thus they saturate poorly. However, due to the usually small inductance value, even a very small absolute estimation error can lead to a significant percent error. To consider this potential mismatch in the motor model, simulations were carried out with several mismatches in the range of $\pm 40\%$ of the nominal value. The mean q–current value and the c_f factor are reported in Fig. 3. As can be seen in Fig. 3a, the induced error on the steady–state q–current is small except for the one–step horizon ($N_p = 1$) case, where it almost reaches 5% with a positive mismatch, i.e., with an overestimated inductance value in the prediction model. On the other hand, a long prediction horizon reduces the error on the generated q–current. Moreover, both the steady–state error and the c_f factor are almost insensitive to the length of the implemented prediction horizon. The steady–state error is almost symmetric with respect to the nominal case, i.e., the steady–state current decreases as the inductance mismatch increases, and vice–versa. Nevertheless, the performance factor c_f shows an asymmetric behavior since an overestimated inductance results in a more significant performance deterioration than an equivalent underestimated one, as also reported in [12].

Based on the above, it can be concluded that the steady–state error and the c_f factor are partially influenced by an inductance mismatch. Despite this, it is preferable to underestimate the inductance value since better control performance can be achieved. Finally, it is worth remembering that the motor inductance decreases as the motor saturates, thus the control condition move towards the most critical situation, namely an inductance value overestimation.

3) Permanent Magnet Analysis: The PM plays a crucial role in a PMSM, in generating both the electromagnetic torque and the back electromotive force (BEMF). In particular, the BEMF constitutes almost all of the voltage to be applied to the motor, thus a PM mismatch will lead a considerable performance degradation. A PM flux linkage error in the model could be due to an initial estimation discrepancy, or to a motor temperature variation. To take into account this variability, the PM error was tested in the range of $\pm 30\%$ of the nominal value and the results are reported in Fig. 4. With an unitary horizon, the current error magnitude is symmetric with respect to the nominal case, i.e., the mean q–current increases as the PM mismatch increases, and vice–versa. As can be observed, the tracking accuracy of MPC considerably deteriorates with both an increasing PM mismatch and prediction horizon length, see Fig. 4a. On the other hand, an underestimated PM value leads to a steady–state current error which is not affected by the prediction horizon. This behavior discrepancy is better observed when the factor c_f is examined, see Fig. 4b. Indeed a smaller PM value in the prediction model results in a smaller MPC performance degradation. As can be seen, c_f increases as both the PM mismatch and the horizon length increase, indicating an unfavorable ratio between current distortions and

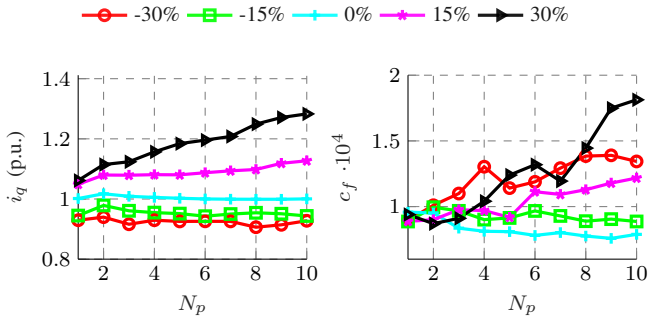

(a) Mean q-current value (b) c_f factor

Fig. 4: Current behaviour and c_f as a function of the prediction horizon N_p, when using FCS-MPC with (constant) $\lambda_u = 0.01$ and different degrees of PM mismatch.

switching frequency, and thus an inferior system performance.

The presented results indicate that the PM is the motor parameter that primarily and deeply affects the FCS–MPC performance. As with the motor inductance, an underestimation of the PM is preferable since the control performance degradation is limited. Finally, it is worth noting that an increase in motor temperature reduces the PM flux linkage, thus the prediction model assumes an overestimated PM value. As a result, the controller moves towards the most critical condition.

B. FCS–MPC Based on the Velocity–Form Prediction Model

A second set of simulations was carried out to assess the effectiveness of the velocity form–based prediction model to the robustness of FCS–MPC. As seen in Section V-A, the most critical condition for the classical MPC scheme happens with a long prediction horizon and significant positive mismatches in all parameters of concern. In light of this, the velocity formulation was evaluated with a ten-step ($N_p = 10$) prediction horizon and the biggest (both positive and negative) mismatches examined in Section V-A for each individual motor parameter. For comparison purposes, the MPC performance without parameter discrepancy is reported as reference. It is worth noting that, despite the additional integrator, the velocity model is equivalent to the classical one when no parameter mismatches exist, thus nominal results are reported without indicating the used implementation. The simulations were carried out with several values of λ_u to achieve a wide range of switching frequencies. Specifically, 200 simulations were carried out with a logarithmic spaced weighting factor in the range $\lambda_u \in [10^{-5}\ 10^{-1.6}]$.

1) Resistance Analysis: As shown in Section V-A1, a discrepancy between the value of the stator resistance used in the prediction model and the actual one has a marginal influence on MPC performance. Fig. 5 presents the MPC performance based on both models and confirms the above-mentioned analysis. The velocity model shows a current reference tracking close to the nominal case and the current distortion is comparable to the classical formulation, as seen in Fig. 5b. Hence, it can be claimed that a mismatch in the stator

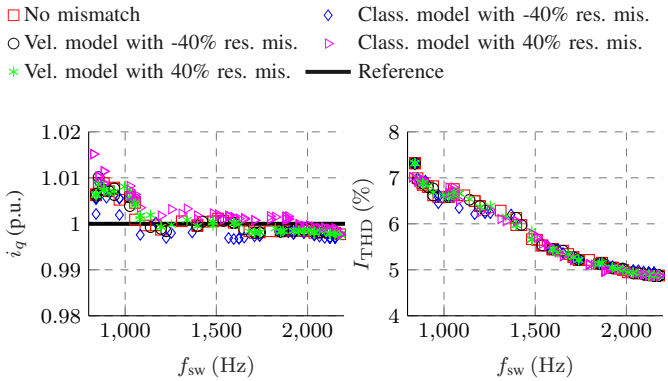

(a) Mean q-current value (b) I_{THD}

Fig. 5: Steady-state current and current THD I_{THD} obtained with FCS–MPC when using either the classical, or the velocity model. A ten-step horizon ($N_p = 10$) is considered and a $\pm 40\%$ resistance mismatch. For comparison purposes, the controller performance with nominal system parameters (i.e., no mismatches) is shown.

resistance does not negatively affect the system performance, regardless of the prediction model employed.

2) Inductance Analysis: Fig. 6 compares the MPC performance with both prediction models and a $\pm 40\%$ inductance mismatch. The FCS–MPC performance with the classical model is slightly worse than the nominal case. The q–current tracking is satisfactory, especially with an overestimated inductance and it is close to the reference case. Despite this, the achievable switching frequency range with the classical model and an inductance mismatch is very different with respect to the nominal case. Indeed a smaller inductance value limits the obtainable switching frequencies to lower frequencies, whereas a bigger one moves the achievable range up.

The velocity model takes this to extremes. A negative inductance mismatch concentrates the obtainable switching frequencies around 900 Hz and an overestimated one shifts the achievable frequency range up by about 1000 Hz compared to the classic MPC model. Furthermore, with a positive inductance mismatch the current distortion increases a lot despite a noticeable increase in switching frequencies. As can be observed in Fig. 6, FCS–MPC with the velocity model performs worse than the classic MPC formulation in terms of current distortions when an inductance mismatch exists, despite the intrinsic integrator. Furthermore, Fig. 7 shows the three-phase stator current and switch position obtained with a weighting factor $\lambda_u = 0.01$ in the previous working condition, for FCS–MPC with either the classical or the velocity model. For a sake of completeness, Table II reports the corresponding switching frequencies and current distortions.

Based on the presented results, it can be deduced that a mismatch in the inductance of the PMSM has a strong negative effect on the performance of FCS–MPC with the velocity form perdiction model. The motor inductance together with the stator resistance define the PMSM electrical time constant

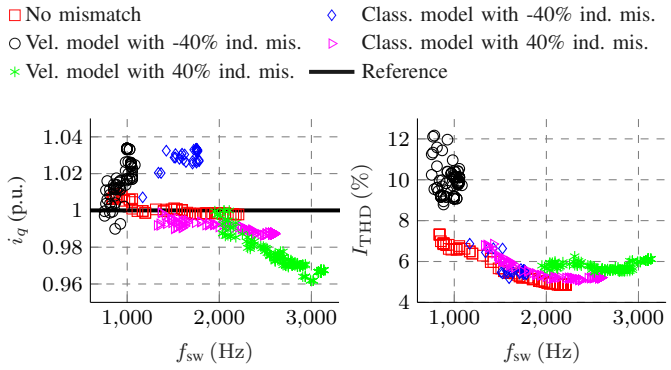

(a) Mean q-current value (b) I_{THD}

Fig. 6: Steady-state current and current THD I_{THD} obtained with FCS-MPC when using either the classical or the velocity model. A ten-step horizon ($N_p = 10$) is considered and a $\pm 40\%$ inductance mismatch. For comparison purposes, the controller performance with nominal system parameters (i.e., no mismatches) is shown.

TABLE II: MPC performance comparison with $\lambda_u = 0.01$.

	Sw. Freq. f_{sw} (Hz)	I_{THD} (%)
Class. model $\Delta L = -40\%$	1.595 kHz	5.36 (%)
Vel. model $\Delta L = -40\%$	1.083 kHz	9.64 (%)
Class. model $\Delta L = 40\%$	1.396 kHz	6.43 (%)
Vel. model $\Delta L = 40\%$	2.094 kHz	5.60 (%)

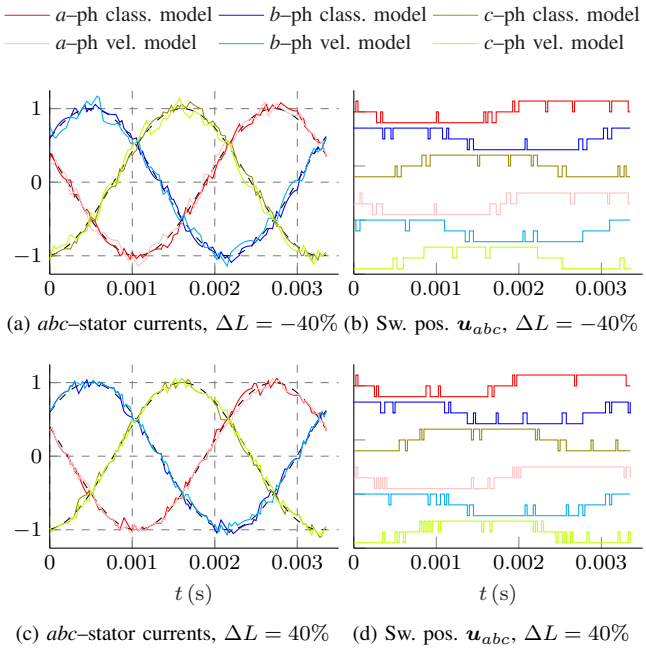

(a) *abc*–stator currents, $\Delta L = -40\%$ (b) Sw. pos. $\boldsymbol{u}_{abc}$, $\Delta L = -40\%$

(c) *abc*–stator currents, $\Delta L = 40\%$ (d) Sw. pos. $\boldsymbol{u}_{abc}$, $\Delta L = 40\%$

Fig. 7: Four simulations of Fig. 6 are reported in time domain. Steady-state currents and switch positions obtained with the classical and the velocity MPC formulation. A ten–step horizon ($N_p = 10$) is considered and a $\pm 40\%$ inductance mismatch. The weighting factor was set $\lambda_u = 0.01$.

which characterizes the dynamic system behavior. Hence, a mismatch between the value used in the prediction model and the actual one compromises the closed-loop stability and performance. The poor performance shown by the velocity model (see Fig. 6b) can be attributed to a limited closed–loop stability. Recalling the classical control theory, an integrator reduces the phase margin, leading the system towards the instability [22]. A similar behavior occurs with MPC based on the velocity form prediction model, which is more sensitive to mismatches appearing in the dynamic matrix $\mathbf{A}$. Nevertheless, an increased system robustness can be achieved by increasing the weighting factor λ_u [23].

3) Permanent Magnet Analysis: The PM is the motor parameter which mostly affects the MPC control performance based on the classical motor model, as analyzed in Section V-A3. Fig. 8 compares the MPC performance with the classical (3) and velocity (11) model for a ten–step horizon ($N_p = 10$) MPC and a $\pm 30\%$ PM mismatch. The classical MPC with a mismatch introduces a significant steady–state current tracking error, while the current harmonic distortions increase with both a positive and negative mismatch. The weighting factor λ_u has no influence on the current tracking accuracy which is almost constant over the whole range of achievable switching frequencies, thus it is only affected by the mismatch magnitude. On the other hand, the velocity model achieves comparable results with the nominal case, adding a high degree of robustness to the FCS–MPC scheme. The only difference is that it cannot reach as low switching frequencies as those in the nominal case.

Interpreting the presented results, and by considering the motor model (3), it can be seen that PM acts as an external disturbance. It does not affect the closed loop stability, as is the case of the motor inductance. Hence, by exploiting the integrator included in the velocity model, the controller can effectively reject the unmodeled disturbance represented by the share of the counter-electromotive force due to the parameter mismatch.

VI. Conclusion

This paper discussed the effects of parameters mismatches on the performance of FCS–MPC for PMSM drive systems. To facilitate this, both positive and negative mismatches were introduced into the prediction model for all motor parameters and the subsequent (adverse) effect on the controller performance was analyzed for different prediction horizons. As shown, due to the absence of an integrating action from the MPC, considerable parameter mismatches can lead to significant performance deterioration. Specifically, at full speed and rated load, the most critical parameter is the PM which can lead to significant performance deterioration, in terms of both current tracking accuracy and current distortions. However, MPC achieves better performance when parameters are underestimated, i.e., the parameter values in the prediction model are smaller than the actual ones.

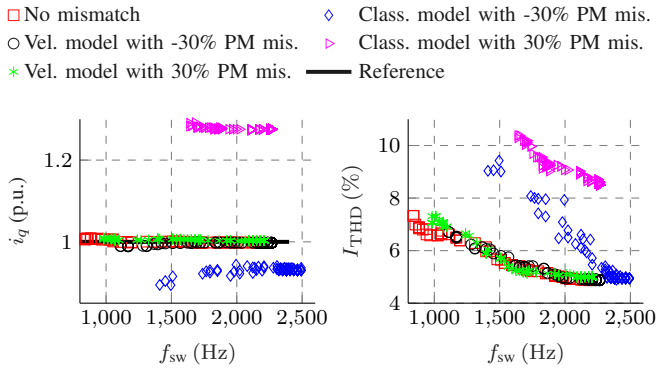

(a) Mean q-current value (b) I_{THD}

Fig. 8: Steady-state current and current THD I_{THD} obtained with FCS-MPC when using either the classical or the velocity model. A ten-step horizon ($N_p = 10$) is considered and a $\pm 30\%$ PM mismatch. For comparison purposes, the controller performance with nominal system parameters (i.e., no mismatches) is shown.

In a second step, and to tackle the performance deterioration due to the parameter mismatches, an alternative system modeling was proposed that adds a high degree of robustness to modeling errors. As shown, the presented modeling adds an integrator to the control problem without augmenting the state. The related robustness analysis indicated that the addition of the integrator improves the system robustness to parameter variations and mismatches, especially with respect to a potential PM discrepancy. Notwithstanding the above, an integrator amplifies a probable inductance mismatch, thus making the controller more sensitive to such deviations. As a result, stability issues may arise.

APPENDIX

$$\boldsymbol{\Gamma} = \begin{bmatrix} \mathbf{A} \\ \mathbf{A} \\ \vdots \\ \mathbf{A}^{N_p} \end{bmatrix}, \quad \mathbf{M} = \begin{bmatrix} \mathbf{I} & \cdots & \mathbf{0} & \mathbf{0} \\ \mathbf{A} & \cdots & \mathbf{0} & \mathbf{0} \\ \vdots & & \vdots & \vdots \\ \mathbf{A}^{N_p-1} & \cdots & \mathbf{A} & \mathbf{I} \end{bmatrix},$$

$$\boldsymbol{\Upsilon} = \mathbf{M} \begin{bmatrix} \mathbf{B} \\ \mathbf{B} \\ \vdots \\ \mathbf{B} \end{bmatrix}, \quad \mathbf{D}(k) = \begin{bmatrix} \boldsymbol{d}(k) \\ \vdots \\ \boldsymbol{d}(k+N_P-1) \end{bmatrix},$$

$$\mathbf{E} = \begin{bmatrix} \mathbf{I} \\ \mathbf{0} \\ \mathbf{0} \\ \vdots \\ \mathbf{0} \end{bmatrix}, \quad \mathbf{S} = \begin{bmatrix} \mathbf{I} & \mathbf{0} & \cdots & \mathbf{0} \\ -\mathbf{I} & \mathbf{I} & \cdots & \mathbf{0} \\ \mathbf{0} & -\mathbf{I} & \cdots & \mathbf{0} \\ \vdots & \vdots & & \vdots \\ \mathbf{0} & \mathbf{0} & \cdots & \mathbf{I} \end{bmatrix}.$$

REFERENCES

[1] P. Cortés, M. P. Kazmierkowski, R. M. Kennel, D. E. Quevedo, and J. Rodríguez, "Predictive control in power electronics and drives," *IEEE Trans. Ind. Electron.*, vol. 55, no. 12, pp. 4312–4324, Dec. 2008.

[2] P. Karamanakos, E. Liegmann, T. Geyer, and R. Kennel, "Model predictive control of power electronic systems: Methods, results, and challenges," *IEEE O. J. Ind. Appl.*, vol. 1, pp. 95–114, 2020.

[3] F. Betin, G. Capolino, D. Casadei, B. Kawkabani, R. I. Bojoi, L. Harnefors, E. Levi, L. Parsa, and B. Fahimi, "Trends in electrical machines control: Samples for classical, sensorless, and fault-tolerant techniques," *IEEE Ind. Electron. Mag.*, vol. 8, no. 2, pp. 43–55, 2014.

[4] P. Karamanakos and T. Geyer, "Guidelines for the design of finite control set model predictive controllers," *IEEE Trans. Power Electron.*, vol. 35, no. 7, pp. 7434–7450, Jul. 2020.

[5] X. Liu, L. Zhou, J. Wang, X. Gao, Z. Li, and Z. Zhang, "Robust predictive current control of permanent-magnet synchronous motors with newly designed cost function," *IEEE Trans. Power Electron.*, vol. 35, no. 10, pp. 10 778–10 788, Oct. 2020.

[6] M. Siami, D. A. Khaburi, A. Abbaszadeh, and J. Rodríguez, "Robustness improvement of predictive current control using prediction error correction for permanent-magnet synchronous machines," *IEEE Trans. Ind. Electron.*, vol. 63, no. 6, pp. 3458–3466, Jun. 2016.

[7] S. Bolognani, S. Bolognani, L. Peretti, and M. Zigliotto, "Design and implementation of model predictive control for electrical motor drives," *IEEE Trans. Ind. Electron.*, vol. 56, no. 6, pp. 1925–1936, Jun. 2009.

[8] A. Bemporad, M. Morari, V. Dua, and E. N. Pistikopoulos, "The explicit linear quadratic regulator for constrained systems," *Automatica*, vol. 38, no. 1, pp. 3–20, Jan. 2002.

[9] L. Ortombina, F. Tinazzi, and M. Zigliotto, "Adaptive maximum torque per Ampere control of synchronous reluctance motors by radial basis function networks," *IEEE J. Emerg. Sel. Topics Power Electron.*, vol. 7, no. 4, pp. 2531–2539, Dec. 2019.

[10] S. J. Underwood and I. Husain, "Online parameter estimation and adaptive control of permanent-magnet synchronous machines," *IEEE Trans. Ind. Electron.*, vol. 57, no. 7, pp. 2435–2443, Jul. 2010.

[11] F. Tinazzi, P. G. Carlet, S. Bolognani, and M. Zigliotto, "Motor parameter-free predictive current control of synchronous motors by recursive least-square self-commissioning model," *IEEE Trans. Ind. Electron.*, vol. 67, no. 11, pp. 9093–9100, Nov. 2020.

[12] H. A. Young, M. A. Perez, and J. Rodríguez, "Analysis of finite-control-set model predictive current control with model parameter mismatch in a three-phase inverter," *IEEE Trans. Ind. Electron.*, vol. 63, no. 5, pp. 3100–3107, May 2016.

[13] X. Zhang, L. Zhang, and Y. Zhang, "Model predictive current control for PMSM drives with parameter robustness improvement," *IEEE Trans. Power Electron.*, vol. 34, no. 2, pp. 1645–1657, Feb. 2019.

[14] P. Karamanakos, T. Geyer, and R. Kennel, "On the choice of norm in finite control set model predictive control," *IEEE Trans. Power Electron.*, vol. 33, no. 8, pp. 7105–7117, Aug. 2018.

[15] G. Betti, M. Farina, and R. Scattolini, "A robust MPC algorithm for offset-free tracking of constant reference signals," *IEEE Trans. Autom. Control*, vol. 58, no. 9, pp. 2394–2400, Sep. 2013.

[16] G. Pannocchia and J. B. Rawlings, "The velocity algorithm LQR: a survey," Technical report, University of Wisconsin-Madison, 2001.

[17] A. Favato, P. G. Carlet, F. Toso, and S. Bolognani, "A model predictive control for synchronous motor drive with integral action," in *Proc. IEEE Ind. Electron. Conf.*, Washington, D.C., USA, Oct. 2018, pp. 325–330.

[18] T. Geyer and D. E. Quevedo, "Multistep finite control set model predictive control for power electronics," *IEEE Trans. Power Electron.*, vol. 29, no. 12, pp. 6836–6846, Dec. 2014.

[19] P. Karamanakos, T. Geyer, and R. Kennel, "Suboptimal search strategies with bounded computational complexity to solve long-horizon direct model predictive control problems," in *Proc. IEEE Energy Convers. Congr. Expo.*, Montreal, QC, Canada, Sep. 2015, pp. 334–341.

[20] F. Stinga and D. Popescu, "Robust model predictive control of an induction motor," in *Proc. Int. Conf. Syst. Theory, Control and Comp.*, Sinaia, Romania, Oct. 2014, pp. 381–386.

[21] R. Antonello, L. Ortombina, F. Tinazzi, and M. Zigliotto, "Online stator resistance tracking for reluctance and interior permanent magnet synchronous motors," *IEEE Trans. Ind. Appl.*, vol. 54, no. 4, pp. 3405–3414, Jul./Aug. 2018.

[22] ——, "Advanced current control of synchronous reluctance motors," in *Proc. IEEE Int. Conf. Power Electron. and Drive Syst.*, Honolulu, HI, USA, Dec. 2017, pp. 1037–1042.

[23] R. P. Aguilera and D. E. Quevedo, "Predictive control of power converters: Designs with guaranteed performance," *IEEE Trans. Ind. Inf.*, vol. 11, no. 1, pp. 53–63, Feb. 2015.